

Journal of Mechanics of Materials and Structures

ON THE NONLINEAR DYNAMICS OF OVAL CYLINDRICAL SHELLS

Syed Muhammad Ibrahim, Badri Prasad Patel and Yogendra Nath

Volume 5, No. 6

June 2010



mathematical sciences publishers

ON THE NONLINEAR DYNAMICS OF OVAL CYLINDRICAL SHELLS

SYED MUHAMMAD IBRAHIM, BADRI PRASAD PATEL AND YOGENDRA NATH

The nonlinear periodic response characteristics of symmetrically and nonsymmetrically excited oval cylindrical shells are investigated using the first order shear deformation theory based finite strip method. The periodic solutions of the governing second order equations of motion are obtained using the shooting technique coupled with Newmark time marching and the arc length continuation algorithm. The effect of ovality parameter and loading locations on the steady state frequency response and modal participation factors is studied. For circular shells ($\zeta = 0.0$), travelling waves emanating at loading point but moving in opposite directions for certain range of forcing frequency are brought out. For the symmetrically excited oval shell with $\zeta = 0.6$, due to 1:1 internal resonance between the AS/SS and SA/AA modes, a secondary branch with traveling wave response emanates from the primary one through a symmetry breaking bifurcation. For the nonsymmetrically excited oval shells ($\zeta = 0.6$), either waves moving in anticlockwise direction or those originating near the major axis and moving in opposite directions in the top and bottom halves of the shell are observed for certain forcing frequency ranges.

A list of symbols can be found on page 907.

1. Introduction

Large amplitude vibrations occur frequently in thin shells and panels used in the aerospace industry, as they are subjected to high acoustic and aerodynamic excitations. For the study of such vibrations, a linear model (usually the first approximation to the actual system) is often inadequate. In particular, the nonlinear forced response analysis of closed circular cylindrical shells still remains an active and challenging area of research [Moussaoui and Benamar 2002; Amabili and Païdoussis 2003; Amabili 2008].

Shells with variable curvature, especially oval and elliptical cylindrical shells, are used in nuclear fusion reactors, heat exchangers, aerospace and underwater structures due to special external shape or internal storage requirements. Noncircularity may also be introduced while fabricating circular shells. The variable stiffness along the circumference of a shell due to noncircularity leads to the coupling of modes with different circumferential wave numbers of a corresponding perfect circular shell and influences the dynamic characteristics significantly. The asymmetric free vibration modes of perfect circular cylindrical shells are not spatially fixed, due to axisymmetric geometry, but noncircular shells with doubly symmetric cross-section have spatially fixed free vibration modes, categorised as AS, SA, SS, AA, the first and second letters indicating symmetry or antisymmetry about the major and minor axes, respectively.

Studies relating to the linear static and dynamic, buckling and nonlinear static analyses of shells with noncircular cross-sections have been reviewed in [Soldatos 1999]. Investigations on the nonlinear

Keywords: noncircular shell, nonlinear, periodic, shooting, travelling wave, internal resonance.
The authors are grateful to DST, India (Project No. SR/S3/MERC/46/2005) for financial support.

vibration characteristics of oval and elliptical shells are quite limited. Using the Galerkin method, [Pandalai and Sathyamoorthy \[1970\]](#) investigated large amplitude flexural vibrations of simply supported thin oval rings and finite oval cylindrical shells using one axisymmetric and one asymmetric term in the approximation of transverse displacement, and a softening type behaviour was found. Using the Bubnov–Galerkin method, the nonlinear free vibration of thin-walled elastic cylindrical shell of elliptic cross-section was analysed in [\[Kozarov and Mladenov 1979\]](#) using a single term approximation of all the three displacements (axial, circumferential, radial) and predicted hardening behaviour. The studies [\[Pandalai and Sathyamoorthy 1970; Kozarov and Mladenov 1979\]](#) are based on approximate analytical solutions that may affect the accuracy of the results. Patel et al. [\[2002; 2003\]](#) investigated the nonlinear free flexural vibration behaviour of the isotropic/laminated orthotropic noncircular rings using the finite element approach and Newmark time marching scheme and reported softening nonlinearity. The nonlinear forced vibration analysis of oval cylindrical shells with different support conditions has been carried out in [\[Ibrahim et al. 2008a; 2008b\]](#) employing the direct time integration approach and only part of the stable branches of the frequency response curves could be captured. Further, it is observed that in the direct integration approach, the convergence to a steady state solution is very slow. In addition, the steady state response can not be ascertained in the direct time integration approaches.

Periodic solutions of nonlinear systems can be obtained by the shooting method. Unlike frequency domain methods, the number of equations does not depend on the number of harmonics. Steady state solutions can be reached in significantly fewer iterations than with direct time integration methods. The shooting method also yields the monodromy matrix, which can be used to predict the stability of the solution. In the traditional shooting approach, the dynamical equations of motion are transformed into first order equations [\[Nayfeh and Balachandran 1994; Padmanabhan and Singh 1995; Sundararajan and Noah 1997; Ribeiro 2004; 2008\]](#), thus increasing computational time as the number of equations is doubled and the banded nature of system of equations is destroyed. This issue is quite important, particularly for systems with many degrees of freedom such as the ones resulting from finite element discretisation. Note that a few-degrees-of-freedom model of a continuous system may not capture a priori unknown modal interactions/phenomena. To the best of the authors' knowledge, the complete frequency response characteristics of oval cylindrical shells have not been dealt with in the literature, nor are there results on the participation of different modes, effect of loading location, internal resonance between AS/SS and SA/AA modes and travelling wave response of noncircular cylindrical shells.

The modified shooting technique coupled with the Newmark time marching and arc length continuation algorithm [\[Patel et al. 2009; Ibrahim et al. 2009; 2010\]](#) is employed to investigate the steady state periodic response of the oval cylindrical shells excited in the neighbourhood of the first AS, SA, SS, and AA linear free vibration modes. The analysis is carried out using the finite strip method based on first order shear deformation theory. The effect of the ovality parameter and loading locations on the steady-state frequency response and modal participation factors is studied. Participation of AS and SS modes in the primary branch of symmetrically excited shells and participation of AS, SA, SS, and AA modes in asymmetrically excited shells is brought out. For symmetrically excited shells, a secondary branch corresponding to significant participation of SA/AA modes in addition to AS/SS modes due to one-to-one internal resonance is reported for the first time. For a certain forcing frequency range, shell response includes waves travelling from the loading point in two opposite directions or in the same direction, depending on the forcing frequency.

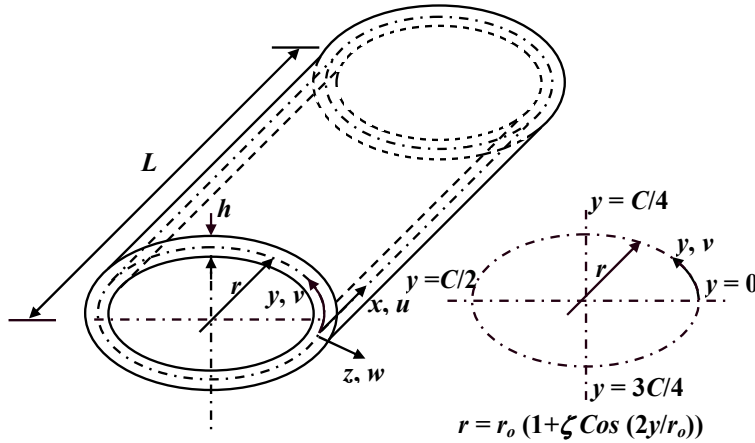


Figure 1. Coordinate system and geometry of oval shell.

2. Formulation

The geometry and coordinate system of the oval cylindrical shell are shown in Figure 1. The coordinates x , y and z having origin at the mid-surface of the shell are considered along the meridional, circumferential and thickness directions, respectively. The displacements u , v , w at a point (x, y, z) , employing the first order shear deformation theory, are expressed as

$$\begin{aligned}
 u(x, y, z, t) &= u_0(x, y, t) + z\theta_x(x, y, t), \\
 v(x, y, z, t) &= v_0(x, y, t) + z\theta_y(x, y, t), \\
 w(x, y, z, t) &= w_0(x, y, t).
 \end{aligned}
 \tag{1}$$

The displacement field variables u_0 , v_0 , w_0 , θ_x and θ_y are represented as the superposition of trigonometric functions in the meridional coordinate x as

$$\begin{aligned}
 u_0(x, y, t) &= \sum_{i=1}^M u_0^i(y, t)U_i(x), \\
 v_0(x, y, t) &= \sum_{i=1}^M v_0^i(y, t)V_i(x), \\
 w_0(x, y, t) &= \sum_{i=1}^M w_0^i(y, t)W_i(x), \\
 \theta_x(x, y, t) &= \sum_{i=1}^M \theta_x^i(y, t)\Theta_{xi}(x), \\
 \theta_y(x, y, t) &= \sum_{i=1}^M \theta_y^i(y, t)\Theta_{yi}(x),
 \end{aligned}
 \tag{2}$$

where the trigonometric functions $U_i(x)$, $V_i(x)$, $W_i(x)$, $\Theta_{xi}(x)$ and $\Theta_{yi}(x)$ satisfying all the boundary conditions for movable simply supported shell at its two ends are taken as in [Soedel 1993]:

$$U_i(x) = \cos(i\pi x/L), \quad V_i(x) = \sin(i\pi x/L), \quad W_i(x) = \sin(i\pi x/L),$$

$$\Theta_{xi}(x) = \cos(i\pi x/L), \quad \Theta_{yi}(x) = \sin(i\pi x/L).$$

For the other boundary conditions, these functions can be chosen appropriately.

The strain-displacement relations are based on kinematic approximations of Sanders type: (i) small strains, (ii) moderately large rotations; and (iii) thin shell ($z/r \ll 1$) such that $1 + z/r \approx 1$. However, transverse shear deformation is important due to smaller wavelength of the deformation shape to thickness ratio. The Green’s strains are written in terms of the midsurface deformations as

$$\boldsymbol{\epsilon} = \left\{ \begin{matrix} \boldsymbol{\epsilon}_p^L \\ \mathbf{0} \end{matrix} \right\} + \left\{ \begin{matrix} z\boldsymbol{\epsilon}_b \\ \boldsymbol{\epsilon}_s \end{matrix} \right\} + \left\{ \begin{matrix} \boldsymbol{\epsilon}_p^{NL} \\ \mathbf{0} \end{matrix} \right\}, \tag{3}$$

where $\mathbf{0}$ is the 2×1 null vector, and

$$\boldsymbol{\epsilon}_p^L = \left\{ \begin{matrix} \frac{\partial u_0}{\partial x} \\ \frac{\partial v_0}{\partial y} + \frac{w_0}{r} \\ \frac{\partial u_0}{\partial y} + \frac{\partial v_0}{\partial x} \end{matrix} \right\}, \quad \boldsymbol{\epsilon}_b = \left\{ \begin{matrix} \frac{\partial \theta_x}{\partial x} \\ \frac{\partial \theta_y}{\partial y} \\ \frac{\partial \theta_x}{\partial y} + \frac{\partial \theta_y}{\partial x} \end{matrix} \right\}, \quad \boldsymbol{\epsilon}_s = \left\{ \begin{matrix} \theta_x + \frac{\partial w_0}{\partial x} \\ \theta_y + \frac{\partial w_0}{\partial y} - \frac{v_0}{r} \end{matrix} \right\}, \quad \boldsymbol{\epsilon}_p^{NL} = \left\{ \begin{matrix} \frac{1}{2} \left(\frac{\partial w_0}{\partial x} \right)^2 \\ \frac{1}{2} \left(\frac{\partial w_0}{\partial y} - \frac{v_0}{r} \right)^2 \\ \frac{\partial w_0}{\partial x} \left(\frac{\partial w_0}{\partial y} - \frac{v_0}{r} \right) \end{matrix} \right\},$$

are respectively the linear membrane, bending, transverse shear, and nonlinear membrane strain vectors, with r the radius of curvature of the oval cylindrical shell, expressed as

$$r = \frac{r_0}{1 + \zeta \cos(2y/r_0)}. \tag{4}$$

The membrane stress resultant $\tilde{\mathbf{N}} = \{N_{xx} \ N_{yy} \ N_{xy}\}^T$, moment resultant $\tilde{\mathbf{M}} = \{M_{xx} \ M_{yy} \ M_{xy}\}^T$ and transverse shear stress resultant $\tilde{\mathbf{Q}} = \{Q_{xz} \ Q_{yz}\}^T$ vectors are related to the membrane $\boldsymbol{\epsilon}_p = \boldsymbol{\epsilon}_p^L + \boldsymbol{\epsilon}_p^{NL}$, bending $\boldsymbol{\epsilon}_b$ and transverse shear $\boldsymbol{\epsilon}_s$ strain vectors through the constitutive relation as

$$\left\{ \begin{matrix} \tilde{\mathbf{N}} \\ \tilde{\mathbf{M}} \end{matrix} \right\} = \begin{bmatrix} \mathbf{A} & \mathbf{B} \\ \mathbf{B} & \mathbf{D} \end{bmatrix} \left\{ \begin{matrix} \boldsymbol{\epsilon}_p \\ \boldsymbol{\epsilon}_b \end{matrix} \right\}, \quad \tilde{\mathbf{Q}} = \mathbf{E} \boldsymbol{\epsilon}_s, \tag{5}$$

where $B_{ij} = 0$ and the nonzero elements of A_{ij} , D_{ij} ($i, j = 1, 2, 6$) and E_{ij} ($i, j = 4, 5$) for an isotropic shell are:

$$A_{11} = A_{22} = \frac{Eh}{1 - \nu^2}, \quad A_{21} = A_{12} = \frac{\nu Eh}{1 - \nu^2}, \quad A_{66} = \frac{Eh}{2(1 + \nu)},$$

$$D_{11} = D_{22} = \frac{Eh^3}{12(1 - \nu^2)}, \quad D_{21} = D_{12} = \frac{\nu Eh^3}{12(1 - \nu^2)}, \quad D_{66} = \frac{Eh^3}{24(1 + \nu)},$$

$$E_{44} = E_{55} = \frac{Eh}{2(1 + \nu)}$$

The potential energy functional U is given by

$$U = \frac{1}{2} \left[\int_A \boldsymbol{\epsilon}_p^T \mathbf{A} \boldsymbol{\epsilon}_p + \boldsymbol{\epsilon}_p^T \mathbf{B} \boldsymbol{\epsilon}_b + \boldsymbol{\epsilon}_b^T \mathbf{B} \boldsymbol{\epsilon}_p + \boldsymbol{\epsilon}_b^T \mathbf{D} \boldsymbol{\epsilon}_b + \boldsymbol{\epsilon}_s^T \mathbf{E} \boldsymbol{\epsilon}_s \right] dA - w_0(L/2, y^*, t)F \tag{6}$$

Based on the approach of [Rajasekaran and Murray 1973], this can be expressed as

$$U(\delta) = \delta^T \left(\frac{1}{2} \mathbf{K} + \frac{1}{6} \mathbf{K}_1(\delta) + \frac{1}{12} \mathbf{K}_2(\delta) \right) \delta - \delta^T \mathbf{F}. \tag{7}$$

The kinetic energy of the shell is given by

$$\tilde{T}(\delta) = \frac{1}{2} \int_A (\gamma (\dot{u}_0^2 + \dot{v}_0^2 + \dot{w}_0^2) + I (\dot{\theta}_x^2 + \dot{\theta}_y^2)) dA \tag{8}$$

where $\gamma = \rho h$ and $I = \rho h^3/12$. The dot over the variables denotes derivative with respect to time.

Substituting (7) and (8) in the Lagrange’s equation of motion and considering dissipative forces, the governing equation of the shell is written as

$$\mathbf{M} \ddot{\delta} + (\alpha \mathbf{M} + \beta \mathbf{K}) \dot{\delta} + \left(\mathbf{K} + \frac{1}{2} \mathbf{K}_1(\delta) + \frac{1}{3} \mathbf{K}_2(\delta) \right) \delta = \mathbf{F}. \tag{9}$$

3. Element description

The field variables in the circumferential direction (y) are approximated using a C^0 continuous three-noded quadratic element and are expressed in terms of their nodal values as

$$(u_0^i, v_0^i, w_0^i, \theta_x^i, \theta_y^i) = \sum_{k=1}^3 \bar{N}_k^0 (u_{0k}^i, v_{0k}^i, w_{0k}^i, \theta_{xk}^i, \theta_{yk}^i), \tag{10}$$

where $\bar{N}_1^0 = (\xi^2 - \xi)/2$, $\bar{N}_2^0 = (1 - \xi^2)$, $\bar{N}_3^0 = (\xi^2 + \xi)/2$; here ξ is the local natural circumferential coordinate of the element and the \bar{N}_k^0 are the original shape functions.

In order to avoid membrane and shear locking, the field redistributed substitute shape functions are used to interpolate the constrained strain fields. These substitute shape functions, obtained using the method of least squares, are

$$\bar{N}_1^1 = \frac{1}{2} \left(\frac{1}{3} - \xi \right), \quad \bar{N}_2^1 = \frac{2}{3}, \quad \bar{N}_3^1 = \frac{1}{2} \left(\frac{1}{3} + \xi \right), \tag{11}$$

where the \bar{N}_i^1 are consistent with $d\bar{N}_i^0/d\xi$.

Using smoothed interpolation functions, the constrained membrane and transverse shear strain components are expressed as

$$\begin{aligned} \frac{\partial v_0}{\partial y} + \frac{w_0}{r} &= \sum_{i=1}^M \sum_{k=1}^3 \left(\frac{\partial \bar{N}_k^0}{\partial y} V_i(x) v_{0k}^i + \bar{N}_k^1 W_i(x) \frac{w_{0k}^i}{r} \right), \\ \frac{\partial u_0}{\partial y} + \frac{\partial v_0}{\partial x} &= \sum_{i=1}^M \sum_{k=1}^3 \left(\frac{\partial \bar{N}_k^0}{\partial y} U_i(x) u_{0k}^i + \bar{N}_k^1 \frac{\partial V_i}{\partial x} v_{0k}^i \right), \\ \theta_y + \frac{\partial w_0}{\partial y} - \frac{v_0}{r} &= \sum_{i=1}^M \sum_{k=1}^3 \left(\bar{N}_k^1 \Theta_{yi}(x) \theta_{yk}^i + \frac{\partial \bar{N}_k^0}{\partial y} W_i(x) w_{0k}^i - \bar{N}_k^1 V_i(x) \frac{v_{0k}^i}{r} \right). \end{aligned} \tag{12}$$

The other strain components are expressed in terms of the original shape functions (\bar{N}_i^0) and their derivatives. The element behaves very well for both thick and thin situations. It has good convergence characteristics and has no spurious rigid body modes [Babu and Prathap 1986].

Integration with respect to the meridional coordinate x is carried out explicitly using Mathematica 5.1. Based on the convergence study for the evaluation of various energy terms, a five-point Gauss-quadrature numerical integration scheme is used with respect to the circumferential coordinate y . Since the element is derived from the field consistency approach, exact integration is performed to evaluate all the energy terms.

4. Solution method

We briefly describe the method used to find periodic solutions to (9). The $2N$ -component state vector $\{\delta(t) \ \dot{\delta}(t)\}^T$ evolves according to (9) from an initial state to be determined. The condition that a solution is periodic with period T is expressed by the equation

$$\begin{Bmatrix} \delta(T) \\ \dot{\delta}(T) \end{Bmatrix} = \begin{Bmatrix} \delta(0) \\ \dot{\delta}(0) \end{Bmatrix} \stackrel{\text{def}}{=} \eta. \tag{13}$$

To find such solutions we use the shooting method. This involves taking a guess for the initial state, integrating the differential equation to the target time T , and then playing with the initial state so as to enforce the periodicity condition (13). To integrate (9) we use Newmark’s direct time integration scheme. To find a satisfactory initial state we use the Newton–Raphson method.

To elaborate, we rewrite (13) stressing the dependence of δ on the initial state vector, and also on the frequency of the forcing term F :

$$\begin{Bmatrix} \delta(T, \eta, \omega_F) \\ \dot{\delta}(T, \eta, \omega_F) \end{Bmatrix} - \eta = \mathbf{0}. \tag{14}$$

Given a first guess η_0 for the initial state vector η , Newton–Raphson tells us to solve the linear system

$$\begin{bmatrix} \left. \frac{\partial \delta(T, \eta, \omega_F)}{\partial \eta} \right|_{\eta=\eta_0} \\ \left. \frac{\partial \dot{\delta}(T, \eta, \omega_F)}{\partial \eta} \right|_{\eta=\eta_0} \end{bmatrix} - \mathbf{I} \Delta\eta_0 = \eta_0 - \begin{Bmatrix} \delta(T, \eta_0, \omega_F) \\ \dot{\delta}(T, \eta_0, \omega_F) \end{Bmatrix} \tag{15}$$

to find the correction $\Delta\eta_0$ to the initial guess. We then repeat the process with $\eta_0 + \Delta\eta_0$ in place of η_0 , and so on, until the equality (14) is satisfied within the desired tolerance limit, which we set at 0.001%. In (15), \mathbf{I} is the $2N \times 2N$ identity matrix and the derivatives $\partial\delta/\partial\eta$ and $\partial\dot{\delta}/\partial\eta$ are $N \times 2N$ matrices. These derivatives are obtained for $t = T$ by applying Newmark’s direct time integration scheme to the differential equation

$$\mathbf{M} \left(\frac{\partial \delta}{\partial \eta} \right)'' + (\alpha \mathbf{M} + \beta \mathbf{K}) \left(\frac{\partial \delta}{\partial \eta} \right)' + (\mathbf{K} + \mathbf{K}_1(\delta) + \mathbf{K}_2(\delta)) \frac{\partial \delta}{\partial \eta} = \mathbf{0}, \tag{16}$$

which is simply the first variation of (9) with respect to η (recall that $K_1(\delta)$ is linear in δ and $K_2(\delta)$ is quadratic). The initial condition for (16), following from the definition of η in (13), is

$$\begin{bmatrix} \partial\delta/\partial\eta \\ \partial\dot{\delta}/\partial\eta \end{bmatrix}_{t=0} = \mathbf{I}. \tag{17}$$

We also calculate the eigenvalues of the monodromy matrix $\begin{bmatrix} \partial\delta/\partial\eta \\ \partial\dot{\delta}/\partial\eta \end{bmatrix}$ using the QR algorithm, in order to study the stability of the periodic response.

We further desire T to be the minimal period. We take T as $2\pi/\omega_F$ for systems with harmonic excitation with angular frequency ω_F , for a response with fundamental and higher harmonics. To obtain the branches of the periodic response curve with subharmonic participation, the response time period T is taken as an integer multiple of fundamental period. For autonomous systems, T is treated as an unknown and an additional equation such as a phase condition/amplitude is required.

For obtaining the complete frequency response, the analysis is carried out in two phases: first, starting far away from resonance, the forcing frequency is incremented and the periodic solutions are obtained; then, when bifurcation points are encountered, the solution is continued via the arc length continuation method. For the second phase, the forcing frequency is treated as an unknown and an incremental arc length is specified.

5. Results and discussion

Validation of the present approach is carried out considering a movable simply supported ($v_0 = w_0 = \theta_y = 0$ at $x = 0, L$) circular cylindrical shell studied by [Amabili 2003]. Dimensions and material properties are: $L = 0.2$ m, $r_0 = 0.1$ m, $\zeta = 0.0$, $h = 0.247$ mm, $E = 71.02$ GPa, $\rho = 2796$ kg/m³, $\nu = 0.31$. Rayleigh proportional damping parameters α and β are determined such that damping factors $\xi_{1,6} = 0.0005$ (corresponding to asymmetric mode with $n = 6$) and $\xi_{1,0} = 0$ (corresponding to axisymmetric mode). The shell is subjected to a point harmonic force at midlength ($x = L/2, y^* = 0$): $F = F_0 \cos(\omega_F t)$, where $F_0 = 0.0785$ N. The first four natural frequencies (ω_{mn}) of the shell corresponding to modes with axial half wave number $m = 1$ and number of circumferential waves $n = 7, 8, 9$ and 6 are found to be 484.38, 489.85, 546.11 and 553.33 Hz, respectively. The forcing frequency (ω_F) is varied in the neighbourhood of the mode with $(m, n) = (1, 6)$ ($\omega_{mn} = 553.33$ Hz). In the approximate solution [Amabili 2003] for transverse displacement w_0 , axisymmetric and asymmetric modes with kn ($k = 1, 2; n = 6$ for this case) circumferential waves were considered. The present results are obtained using a half-wave model of the shell along the circumference, with symmetry conditions at $y = 0, \pi r_0/n$, and the full model. In the half wave model, the participation of axisymmetric and asymmetric modes with kn circumferential waves can

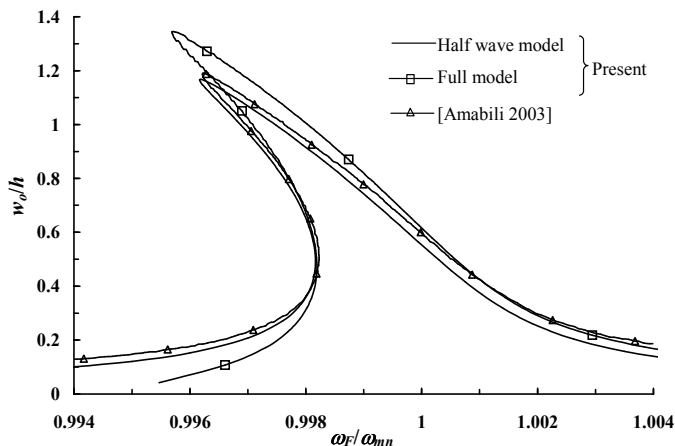


Figure 2. Comparison of steady state response for movable simply supported circular cylindrical shell.

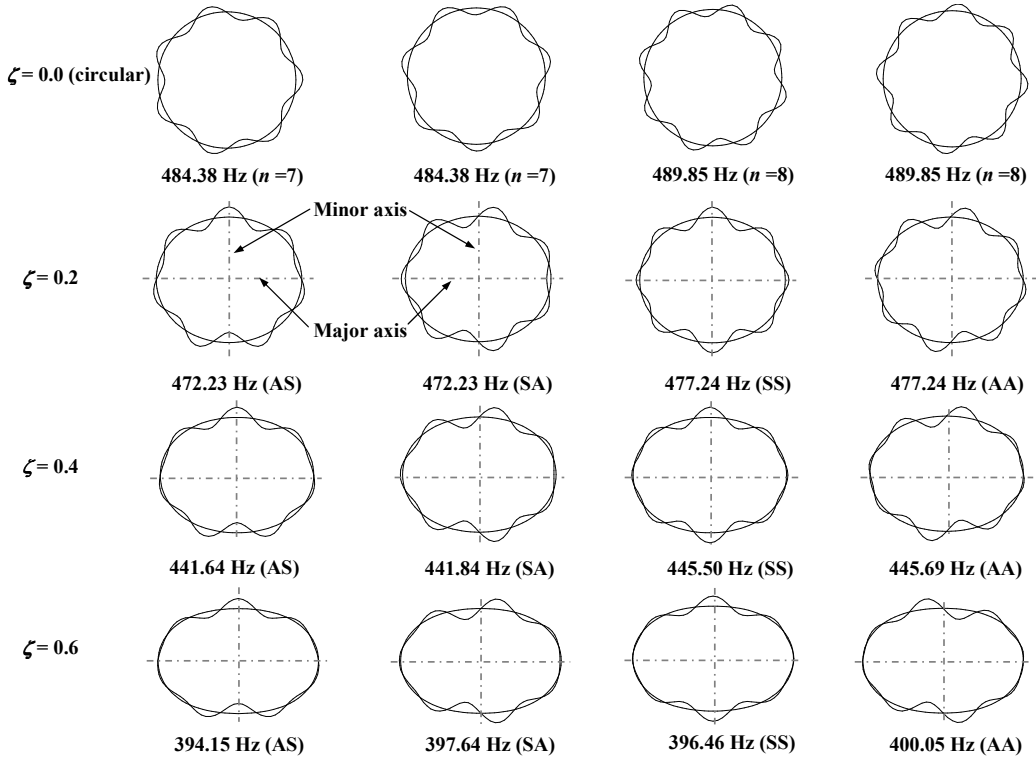


Figure 3. First four free vibration modes and corresponding frequencies of oval cylindrical shells.

be simulated. In the full model, the complete circumferential length of the shell is modelled and it can simulate the participation of all modes with appropriate discretization. The comparison of the results is given in Figure 2. The present results based on the half-wave model are found to be in good agreement with those of [Amabili 2003]. Those based on the full model are slightly different due to the additional participation of the mode with $n = 9$, which is excluded by Amabili and in the present half-wave model.

Next, a detailed study is carried out for different values of the ovality parameter, keeping the other shell parameters the same as in the validation example. The damping parameter α is taken as zero and β is determined such that $\xi_{1,n} = 0.004$. The shell is subjected to a discrete harmonic force ($F = F_0 \cos \omega_F t$) at $y^* = C/4$ for symmetric excitation about the minor axis and at $y^* = 3C/16, C/8, C/16$ for nonsymmetric excitation. The forcing frequency ω_F is varied in the neighbourhood of linear free vibration frequencies corresponding to first SS, SA, AS, AA modes (S = symmetric, A = antisymmetric; major axis symmetry listed first). The free vibration modes and corresponding frequencies of oval cylindrical shells considered in the present study are given in Figure 3. Note that the asymmetric free vibration modes of circular ($\zeta = 0$) cylindrical shells are not spatially fixed due to axisymmetric geometry and there are two modes corresponding to each frequency. Noncircular shells with doubly symmetric cross-section have spatially fixed free vibration modes.

The modal participation factors $\eta_j(t)$ are obtained from $w(x, y, t) = \sum_{j=1}^{\infty} \eta_j(t)\phi_j(x, y)$; where $\phi_j(x, y)$ is the j -th free vibration mode of the oval cylindrical shell. The total response at any location

can be expressed as a Fourier series: $w(x, y, t) = A_0 + \sum_{i=1}^{\infty} A_i \cos(\omega_i t + \psi_i)$, where A_i is the harmonic amplitude, ω_i is a multiple of forcing frequency ω_F , and ψ_i is the phase difference.

A convergence study reveals that $\Delta t = \pi/(100\omega_F)$, $M = 3$, and 48-element discretization in the circumferential direction (total number of degrees of freedom, $N = 960$), are sufficient to yield results of the desired accuracy.

For symmetric loading of circular and oval shells, the travelling wave direction will depend upon the initial conditions. The solutions in the present work are obtained using the shooting technique with initial state vector as the solution of previous frequency step. This has resulted in the traveling wave directions indicated.

The stable regions of loading point response (w_0/h) versus forcing frequency (ω_F/ω_{mn}) characteristics are shown by continuous curves and unstable ones are shown by dashed curves. The bifurcation points marked in the response curves are identified as period doubling (PD) if at least one eigenvalue of the monodromy matrix crosses the unit circle along the negative real axis, as symmetry breaking (SB) / turning point (TP) if it leaves the unit circle along the positive real axis, and as secondary Hopf (SH) bifurcation if a pair of complex conjugate eigenvalues crosses the unit circle.

5.1. Response of symmetrically excited cylindrical shells (load at $y^* = C/4$). The frequency response curves of movable simply supported oval cylindrical shells ($F_0 = 0.4 \text{ N}$, $y^* = C/4$) are shown in Figure 4 for different ovality parameters ($\zeta = 0.0, 0.2, 0.4$ and 0.6). We see that with the increase in the ovality parameter, the nonlinear dynamic response changes significantly due to increased modal interactions and the frequency range corresponding to greater response amplitudes increases. For circular shells ($\zeta = 0.0$), no unstable regions are observed, whereas response of noncircular shells reveals the presence of bifurcation points and unstable regions. The forcing frequency parameter ω_F/ω_{mn} corresponding to

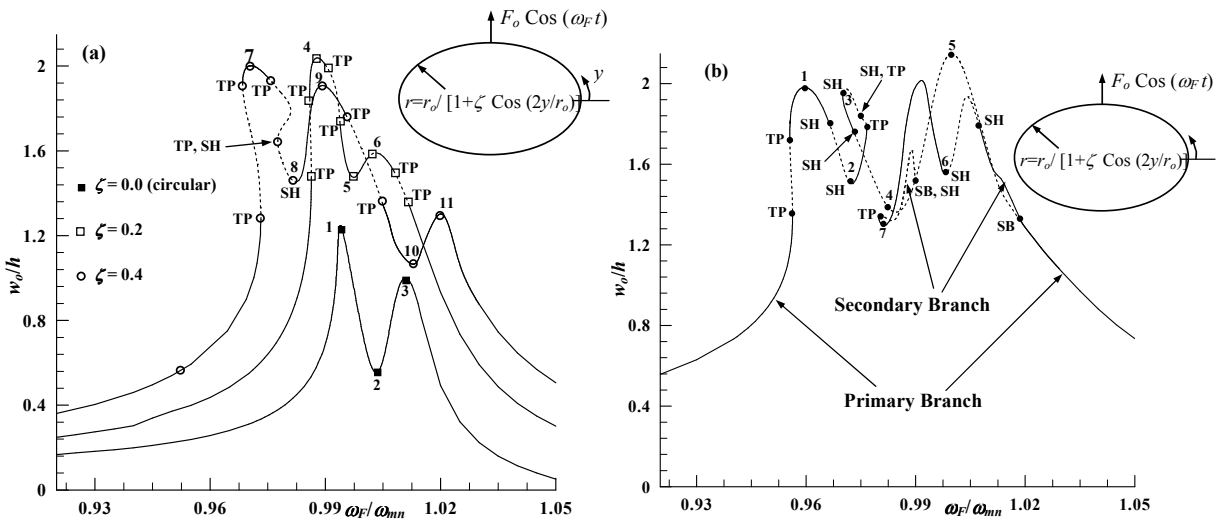


Figure 4. Nonlinear steady state response amplitude versus forcing frequency curves for movable simply supported cylindrical shells subjected to excitation in the neighbourhood of first mode: (a) $\zeta = 0.0$ (circular, $\omega_{mn} = 484.38 \text{ Hz}$), $\zeta = 0.2$ ($\omega_{mn} = 472.23 \text{ Hz}$), and $\zeta = 0.4$ ($\omega_{mn} = 441.64 \text{ Hz}$); (b) $\zeta = 0.6$ ($\omega_{mn} = 394.15 \text{ Hz}$).

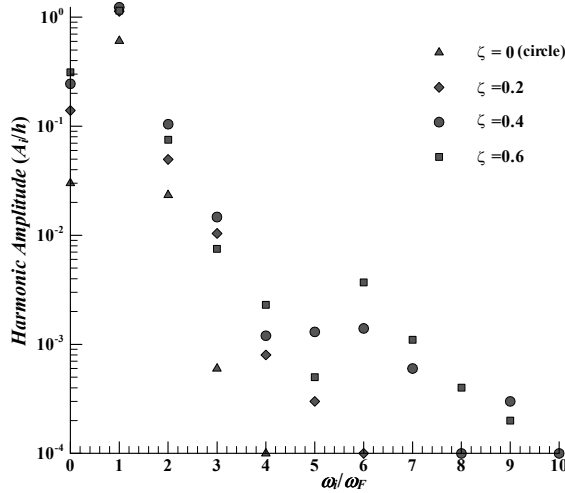


Figure 5. Frequency spectra of oval cylindrical shells with different ovality parameters corresponding to the first peaks of response curves (Figure 4).

first peak response decreases as the ovality parameter increases. The frequency response spectra plotted in Figure 5 corresponding to first peaks of the response curves (Figure 4) reveal that with an increase in the ovality parameter, the number of significant higher harmonics present in the response increases. In particular, the number of higher harmonics is three for $\zeta = 0.0$, five for $\zeta = 0.2$, and up to nine harmonics for $\zeta = 0.4, 0.6$.

The modal participation factors of the first four predominant modes are shown in Figure 6, corresponding to the points marked in Figure 4 for $\zeta = 0.0$. It can be noted from Figure 6 that the participation of the

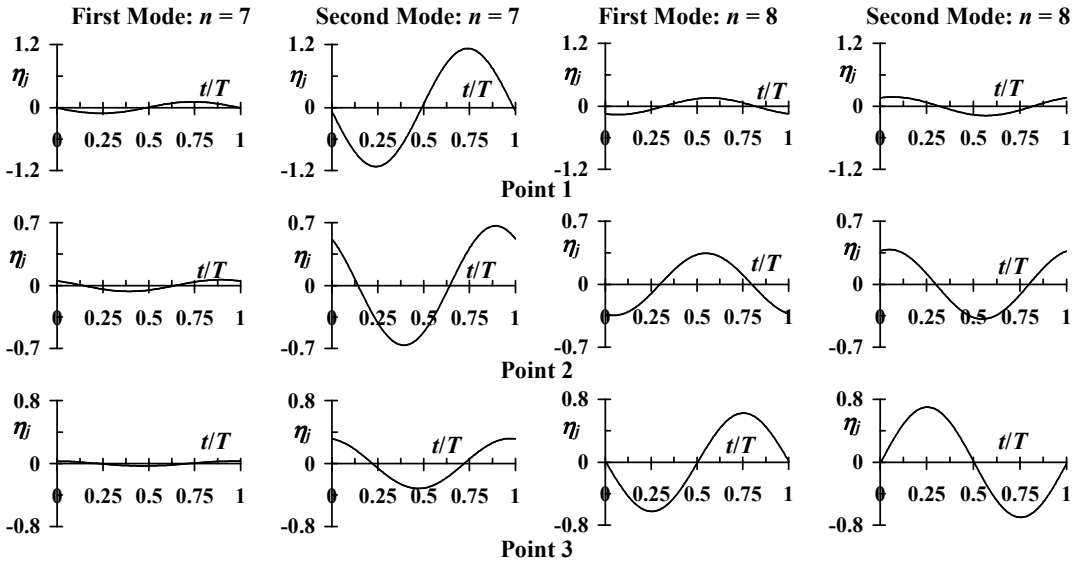


Figure 6. Modal participation factors of the first four modes corresponding to typical points marked (Figure 4a) on the response curves of circular shells ($\zeta = 0.0$).

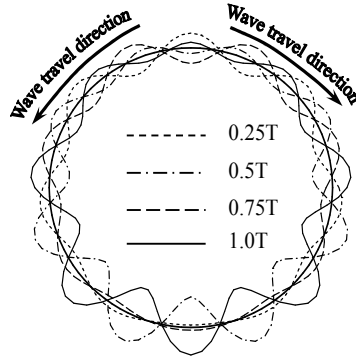


Figure 7. Transverse displacement variations along the circumference at different time instants of one cycle corresponding to point 2 (Figure 4a) on the response curve of circular cylindrical shell ($\zeta = 0.0$).

mode with $n = 7$ is predominant at the first response peak ($w_0/h = 1.24$, $\omega_F/\omega_{mn} = 0.994$) and decreases as the forcing frequency increases further. The participation of the mode with $n = 8$ increases with the forcing frequency and is predominant at point 3 ($w_0/h = 1.00$, $\omega_F/\omega_{mn} = 1.011$). These two modes ($n = 7$ and 8), whose linear free vibration frequencies are very close, are excited due to the concentrated harmonic excitation force.

The deformed shape of the shell cross-section at $x = L/2$ at different moments of one cycle corresponding to point 2 ($w_0/h = 0.55$, $\omega_F/\omega_{mn} = 1.003$) is plotted in Figure 7, revealing waves travelling in two opposite directions from the loading point. This phenomenon is observed for the narrow frequency range between points 1 and 3 due to the participation of modes with $n = 7$ and 8 .

A detailed analysis of the modal participation factors for oval shells reveals that only AS and SS modes participate in the response corresponding to the primary branch of symmetrically excited shells

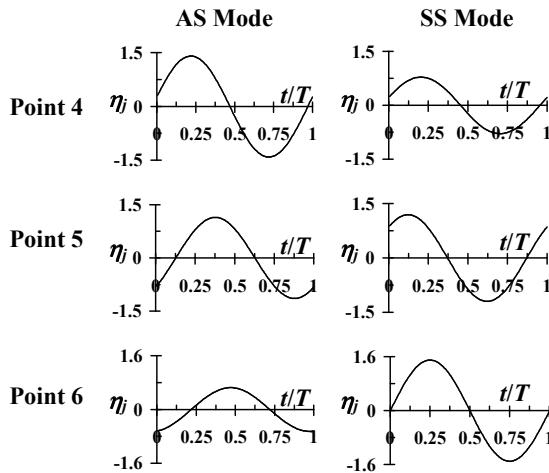


Figure 8. Modal participation factors of the first AS and SS modes for typical points marked (Figure 4a) on the response curve of oval cylindrical shell ($\zeta = 0.2$).

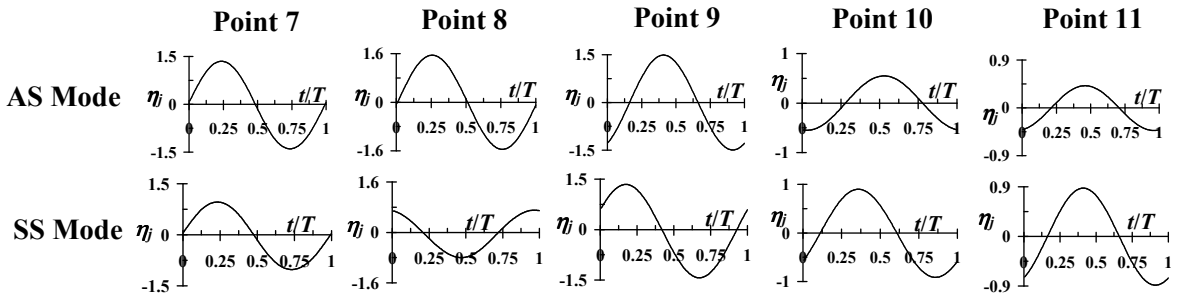


Figure 9. Modal participation factors of the first AS and SS modes corresponding to typical points marked on the response curve of oval cylindrical shell ($\zeta = 0.4$, [Figure 4a](#)).

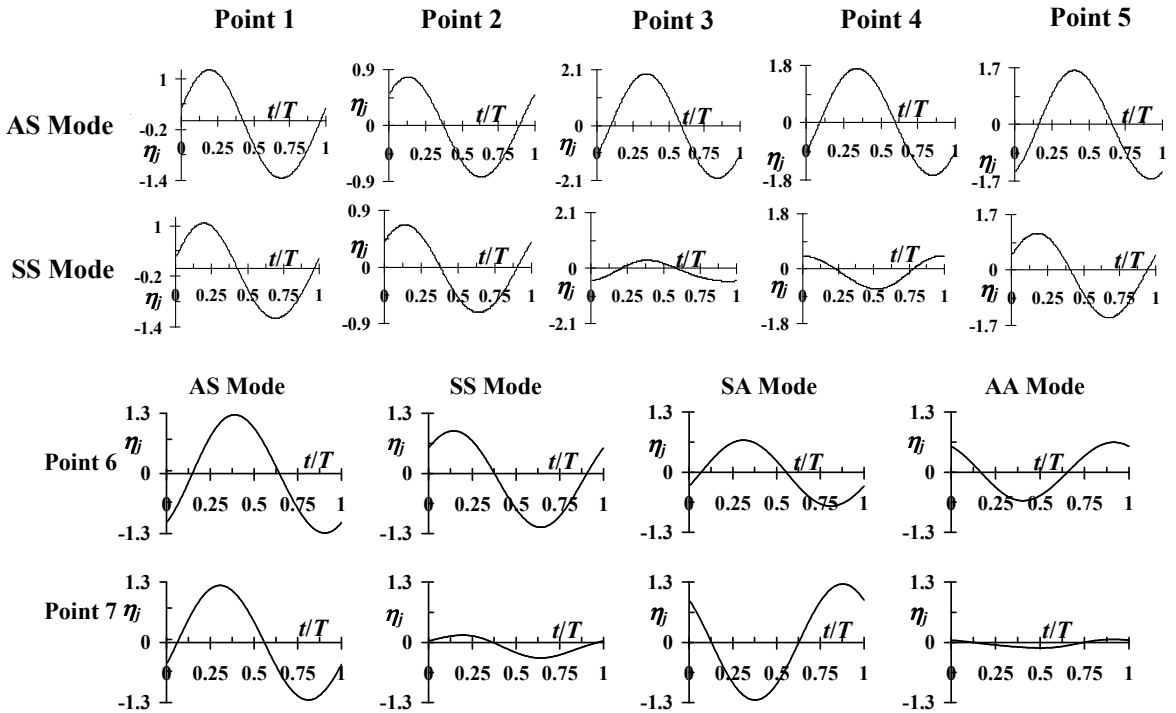


Figure 10. Modal participation factors of the first four modes corresponding to typical points marked on the response curve of oval cylindrical shell ($\zeta = 0.6$, [Figure 4b](#)).

($y^* = C/4$). The modal participation of the first AS and SS modes is shown in [Figure 8](#) and [Figure 9](#) for oval shells with $\zeta = 0.2$ and 0.4 , respectively, corresponding to the points marked in [Figure 4](#). It can be seen from [Figure 8](#) that at the first peak (point 4: $w_0/h = 2.04$, $\omega_F/\omega_{mn} = 0.988$) for $\zeta = 0.2$, the participation of the first AS mode is significantly greater than that of the first SS mode, whereas at the second peak (point 6: $w_0/h = 1.59$, $\omega_F/\omega_{mn} = 1.004$) the opposite trend is observed. At point 5 ($w_0/h = 1.48$, $\omega_F/\omega_{mn} = 0.997$), the participation of both the modes is of comparable amplitude. It can be seen from [Figure 9](#) for $\zeta = 0.4$ that the participation of AS and SS modes at the first (point 7: $w_0/h = 2.00$,

$\omega_F/\omega_{mn} = 0.971$) and last (point 11: $w_0/h = 1.30$, $\omega_F/\omega_{mn} = 1.020$) peaks is qualitatively similar to that for $\zeta = 0.2$. At point 9 ($w_0/h = 1.91$, $\omega_F/\omega_{mn} = 0.989$), the participation of both the modes is comparable. The participation of AS mode is dominant at point 8 ($w_0/h = 1.45$, $\omega_F/\omega_{mn} = 0.982$) and that of SS mode at point 10 ($w_0/h = 1.07$, $\omega_F/\omega_{mn} = 1.013$). In general, it can be concluded that the relative participation of AS mode decreases and that of SS mode increases with the increase in the forcing frequency.

The steady state response amplitude versus forcing frequency curve plotted in Figure 4b for the shell with $\zeta = 0.6$ shows that different response peaks appear at almost equal response amplitudes unlike for $\zeta = 0.4$. The modal participation of the first AS and SS modes is shown in Figure 10 corresponding to the points marked in Figure 4b. It is seen from Figure 10 that at the first peak (point 1: $w_0/h = 1.98$, $\omega_F/\omega_{mn} = 0.960$), the contribution of both AS and SS modes is comparable. From point 1 to 2 (point 2: $w_0/h = 1.50$, $\omega_F/\omega_{mn} = 0.972$), the response amplitude decreases but the relative participation of the AS and SS modes remains the same. From point 2 to 3 (point 3: $w_0/h = 1.97$, $\omega_F/\omega_{mn} = 0.971$), the participation of AS mode increases significantly. The relative participation of the SS mode is very less from point 3 to 4 (point 4: $w_0/h = 1.36$, $\omega_F/\omega_{mn} = 0.985$). After point 4, the response amplitude increases and the curve loses stability through a symmetry breaking bifurcation and the main branch forms peak at point 5 ($w_0/h = 2.15$, $\omega_F/\omega_{mn} = 1.0$), where the contribution of both AS and SS modes is dominant.

The secondary branch emanating from the primary one at the symmetry breaking bifurcation corresponds to a significant participation of the SA and AA modes in addition to the AS and SS modes, as evident from the modal participation factors corresponding to points 6 ($w_0/h = 1.56$, $\omega_F/\omega_{mn} = 0.998$) and 7 ($w_0/h = 1.29$, $\omega_F/\omega_{mn} = 0.981$) shown in Figure 10. This is due to 1:1 internal resonance between AS/SS and SA/AA modes: the ratios of their linear free vibration frequencies are almost equal to one. The multiple peaks depicted in the secondary branch are due to increases/decreases in the relative participation of AS, SA, SS and AA modes. The deformed shape of the shell cross-section at $x = L/2$ at different moments in one cycle corresponding to the point 7 is plotted in Figure 11, showing waves travelling in one direction only.

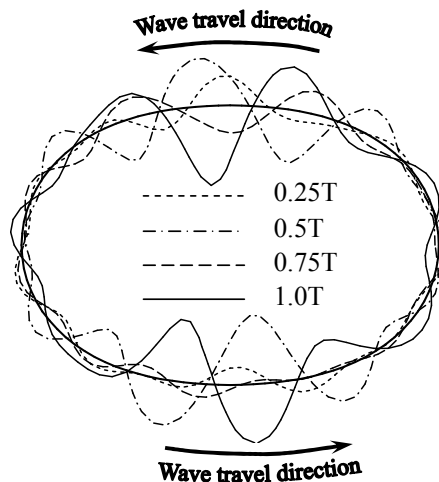


Figure 11. Transverse displacement variations along the circumference at different time instants of one cycle corresponding to point 7 (Figure 4b) on the response curve of oval shell ($\zeta = 0.6$).

To demonstrate the participation of all the modes corresponding to first peak for $\zeta = 0.6$ (point 1 marked in Figure 4b), the modal displacement variations along the circumference and corresponding modal participation factors with time are shown in Figures 12 and 13. It can be seen from Figure 13 that

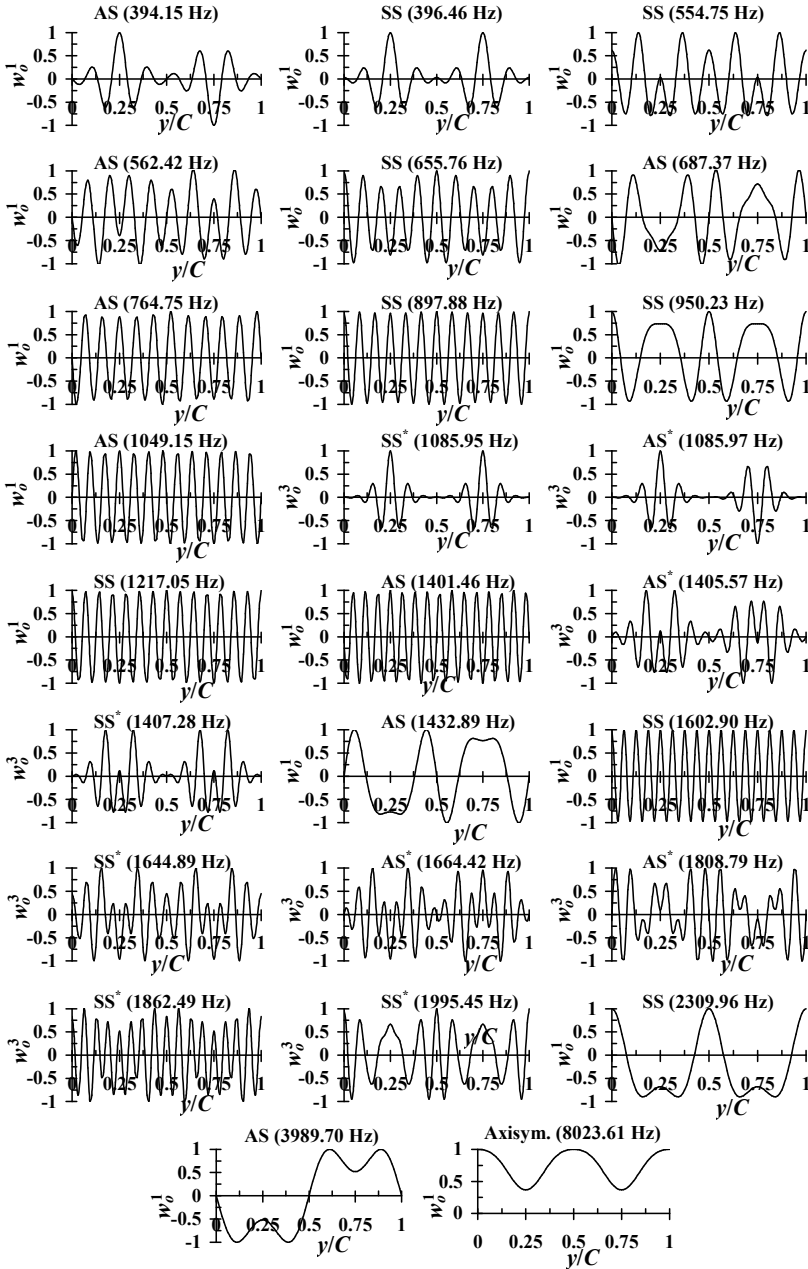


Figure 12. Modal displacement variation along the circumference of the modes participating in the response corresponding to point 1 (Figure 4b) on the response curve of oval cylindrical shell ($\zeta = 0.6$).

in addition to the first AS and SS modes, the other modes participate in the response with fundamental and higher harmonics. Further, due to the harmonic excitation at $(x, y^*) = (L/2, C/4)$, only AS/SS modes, not AA/SA modes, participate in the response corresponding to the primary branch.

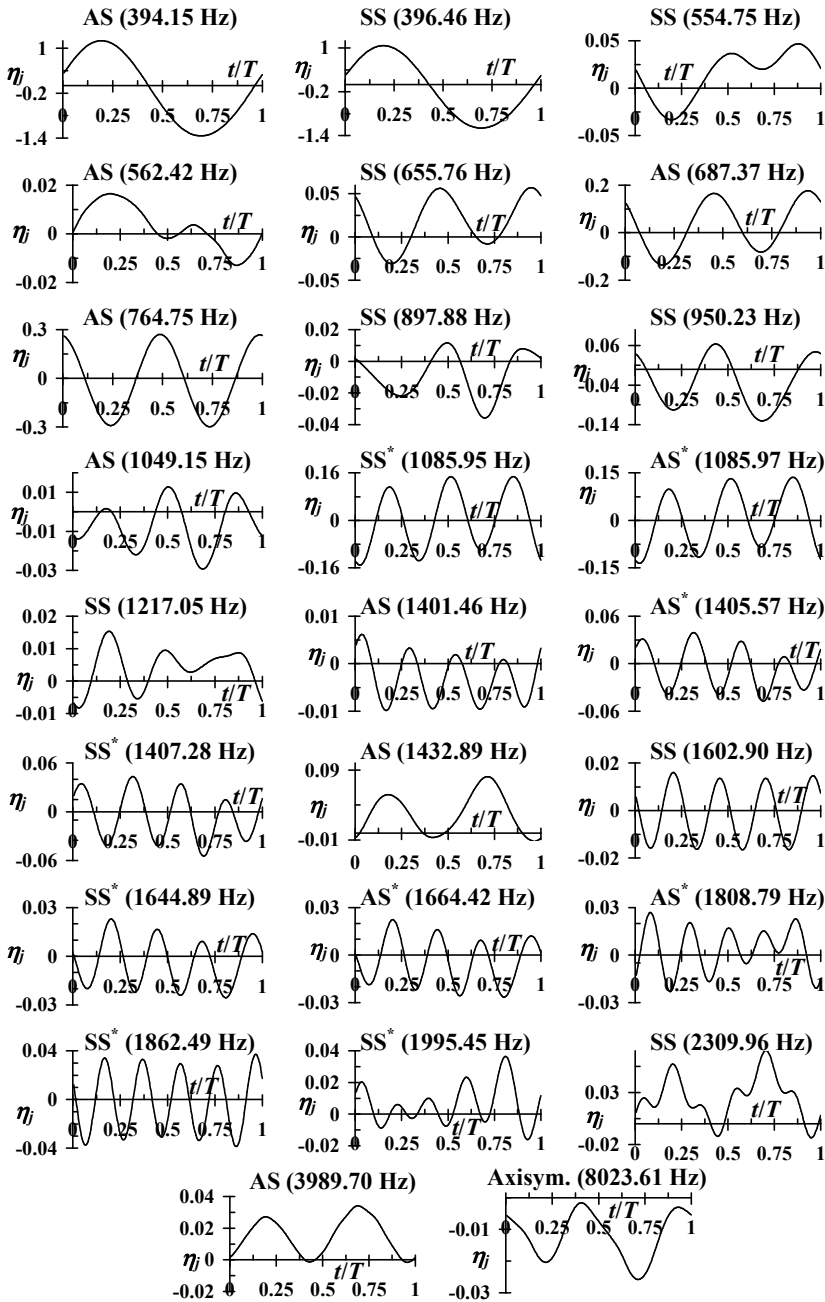


Figure 13. Modal participation factors in the response corresponding to point 1 marked (Figure 4b) on the response curve of oval cylindrical shell ($\zeta = 0.6$).

5.2. Response of nonsymmetrically excited cylindrical shells. The frequency response characteristics of oval shells are investigated by varying the location of the concentrated harmonic excitation force along the circumference. The steady state response amplitude of the loading location versus forcing frequency curves are shown in Figure 14 for oval cylindrical shells with $\zeta = 0.2$ subjected to a concentrated harmonic loading at $y^* = C/4, 3C/16, C/8$ and $C/16$ with the forcing frequency in the neighbourhood of the first AS, SS, SA, and AA modes. The maximum response for the loading locations $y^* = 3C/16, C/8$ and $C/16$ is smaller than that corresponding to the loading at the minor axis ($y^* = C/4$). The modal participation factors of the first four participating modes corresponding to the typical points, marked in Figure 14 on the nonlinear steady state response amplitude versus forcing frequency curves, are shown in Figure 15.

In the response of nonsymmetrically excited oval shells, all types of modes (AS, SS, SA, AA) participate, unlike the primary branch of symmetrically excited shells. The frequency response curve for the shell with $\zeta = 0.2$ (load at $y^* = 3C/16$) shows an unstable region between turning points and a maximum response amplitude of $w_0/h = 1.72$ at $\omega_F/\omega_{mn} = 0.989$ (point 1). The modal participation factors obtained at the peak reveal that the contribution of the AS mode is around 70% of the total response amplitude. The contributions of the SA, SS and AA modes are around 64%, 40% and 40% of the AS mode contribution, respectively. It is also seen that the AS, SS and AA modes are almost in same phase, whereas the SA mode participates with opposite phase. With a further increase in the forcing frequency, the response amplitude decreases, as does the participation of the AS, SS and AA modes. However, the participation of the SA mode increases and at point 2 ($w_0/h = 1.41$, $\omega_F/\omega_{mn} = 0.994$) it becomes around 95% of the AS mode participation. Beyond point 2, another turning point bifurcation is encountered and at point 3 ($w_0/h = 1.40$, $\omega_F/\omega_{mn} = 0.994$), the contribution of AS mode is predominant. After point 3, the relative contribution of the SS mode increases and is maximum at point 4 ($w_0/h = 1.18$, $\omega_F/\omega_{mn} = 0.998$). At the local peak formed at point 5 ($w_0/h = 1.31$, $\omega_F/\omega_{mn} = 1.004$), the contribution

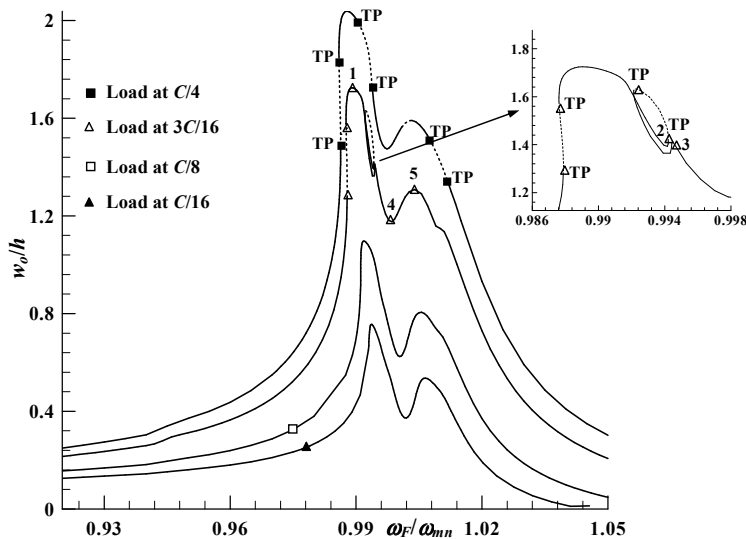


Figure 14. Nonlinear steady state response amplitude versus forcing frequency curves of movable simply supported oval shells subjected to excitation at different circumferential locations in the neighbourhood of the first mode ($\zeta = 0.2$: $\omega_{mn} = 472.23$ Hz).

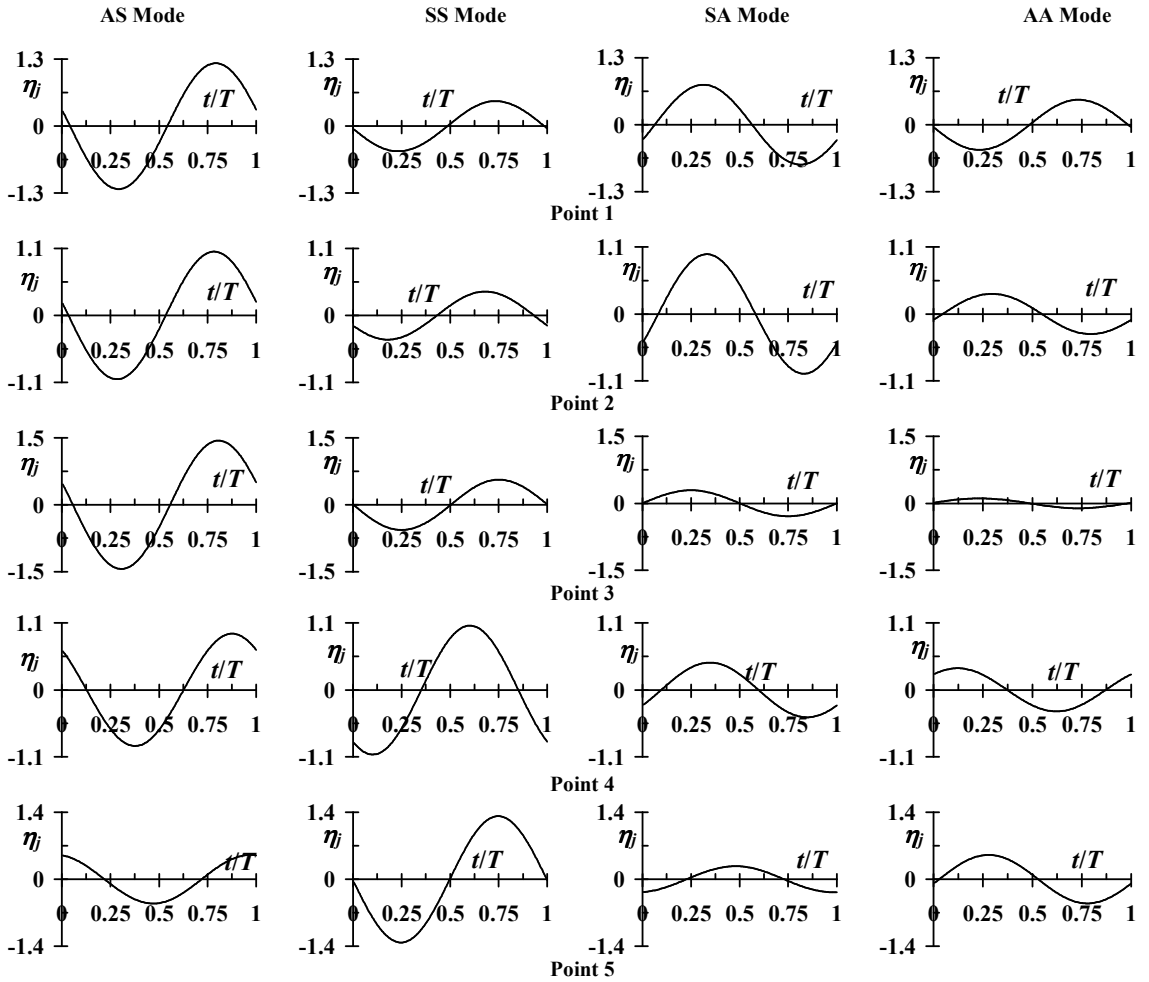


Figure 15. Modal participation factors of the first AS, SS, SA and AA modes corresponding to typical points marked (Figure 14) on the response curve of oval cylindrical shell ($\zeta = 0.2$).

of the SS mode is almost three times the AS mode participation. Further, with the shifting of the loading location towards the major axis, the response amplitude and number of peaks decrease.

The effect of the loading location on the nonlinear steady state response amplitude versus forcing frequency for the shell with $\zeta = 0.6$ is shown in Figure 16. Starting from a low frequency excitation ($\omega_F/\omega_{mn} = 0.925$), the response curve for the loading at $y^* = 3C/16$ loses its stability through a turning point and forms a peak in the unstable region at point 1 ($w_0/h = 1.18$, $\omega_F/\omega_{mn} = 0.979$). This region corresponds to the vibration of the shell predominantly in the AS mode, as seen from the modal participation factors plotted in Figure 17. The relative participations of the SA, SS and AA modes are around 35%, 35% and 15% of the AS mode, respectively.

After point 1, the response amplitude decreases and encounters a secondary Hopf bifurcation, then it increases, becomes stable and forms another peak at point 2 ($w_0/h = 1.43$, $\omega_F/\omega_{mn} = 0.991$). The

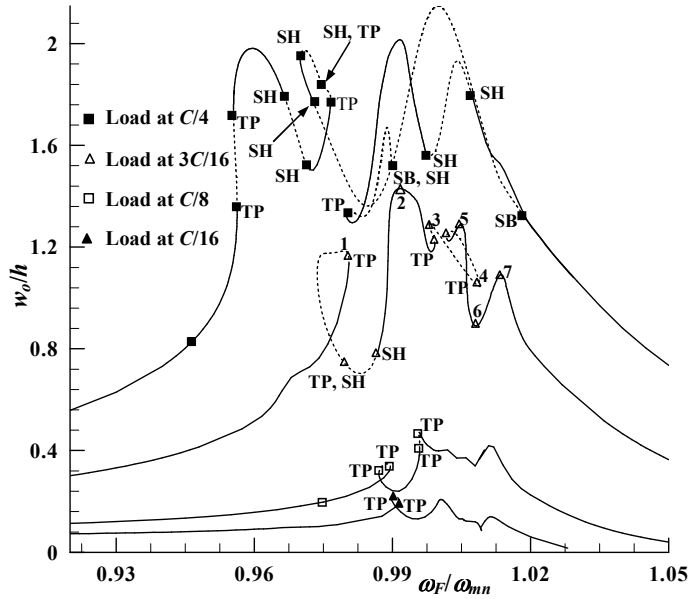


Figure 16. Nonlinear steady state response amplitude versus forcing frequency curves of movable simply supported oval shells subjected to excitation at different circumferential locations in the neighbourhood of the first mode ($\zeta = 0.6$: $\omega_{mn} = 394.15$ Hz).

participation of the first AS, SA, SS and AA modes is significant at this point, with the AS mode having highest participation.

With a further increase in the forcing frequency after point 2, both the relative and the absolute participation of the AS mode decrease and at point 3 ($w_0/h = 1.29$, $\omega_F/\omega_{mn} = 0.998$), its contribution becomes even smaller than that of the SA and SS modes. The participation of the AS and AA modes is around 65% of the SA mode. In the narrow frequency range of $\omega_F/\omega_{mn} = 0.999$ to 1.009, both the absolute and the relative contribution of AA mode first increase and it reaches a peak at point 4 ($w_0/h = 1.05$, $\omega_F/\omega_{mn} = 1.009$), where the next significant mode is SS.

After point 4, the contribution of the AA mode decreases and that of the SS and SA modes increases significantly. At point 5 ($w_0/h = 1.29$, $\omega_F/\omega_{mn} = 1.006$), the relative contribution of the SA mode is greatest, with the participation of the SS, AS and AA modes around 86%, 38% and 30% of SA mode participation.

After point 5, the participation of the AS mode increases and forms a peak at point 6 ($w_0/h = 0.89$, $\omega_F/\omega_{mn} = 1.008$). Subsequently, its relative participation decreases and is least at point 7 ($w_0/h = 1.09$, $\omega_F/\omega_{mn} = 1.014$). From points 6 to 7, the absolute contribution of the SA and SS modes remain almost constant, whereas the contribution of the AA mode increases significantly.

The transverse displacement variations along the circumference at different time instants of one cycle of response corresponding to points 1 and 3 on the response curve are plotted in Figure 18. At point 1, a travelling wave with the significantly greater amplitudes in the upper half of the shell is predicted. At point 3, the travelling waves originating near major axis ($y = 0$) move in opposite directions in the top and bottom halves of the shell with greater amplitude near the minor axis.

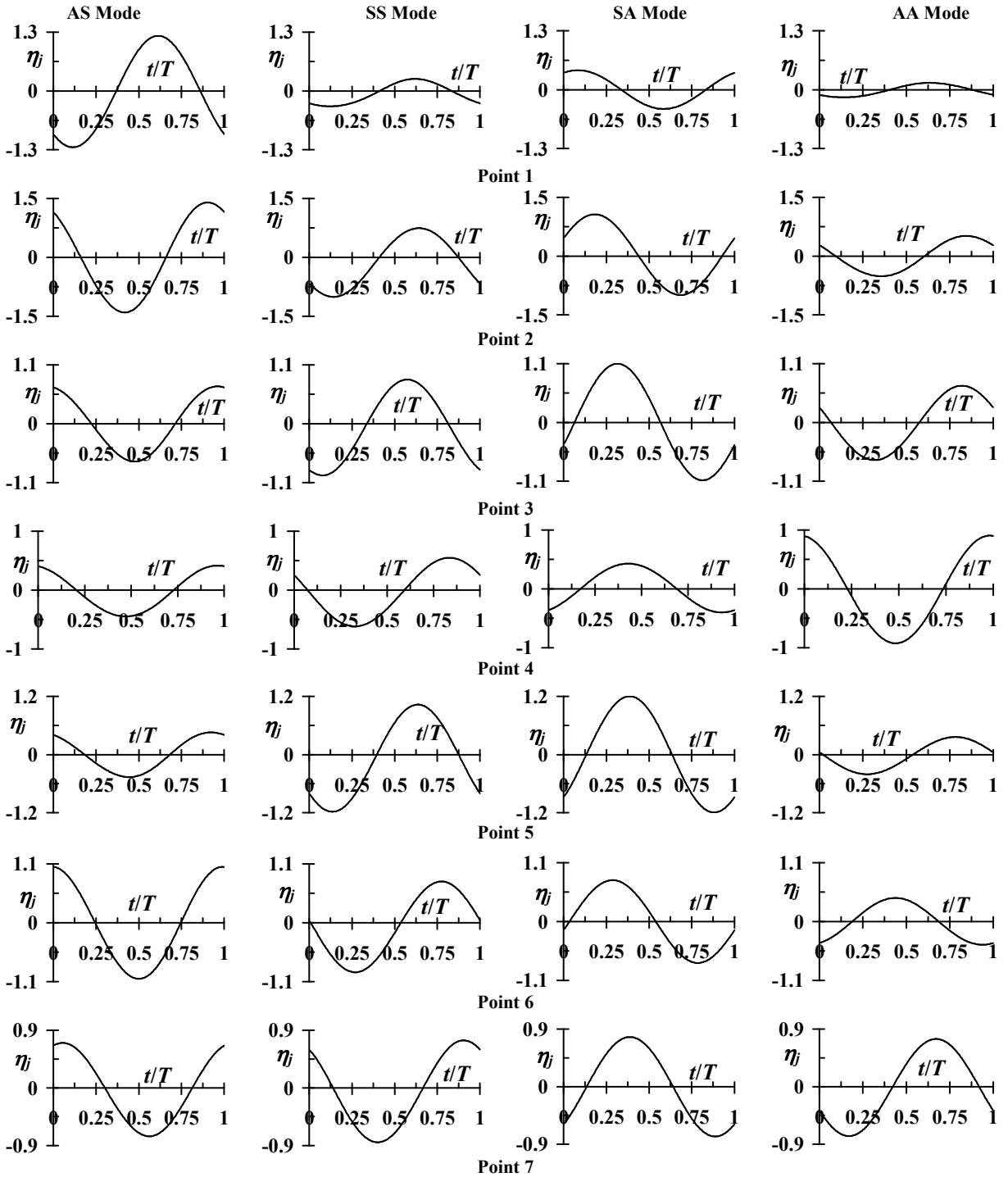


Figure 17. Modal participation factors of the first AS, SS, SA and AA modes corresponding to typical points marked (Figure 16) on the response curve of oval cylindrical shell ($\zeta = 0.6$).

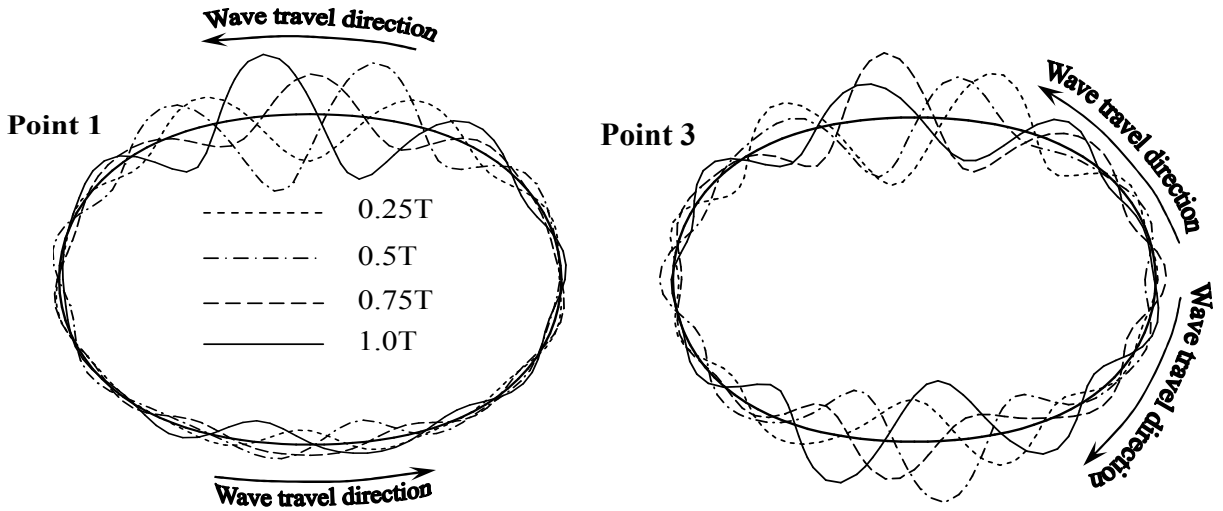


Figure 18. Transverse displacement variations along the circumference at different time instants of one cycle corresponding to points 1 and 3 (Figure 16) on the response curve of oval shell ($\zeta = 0.6$).

6. Conclusions

The nonlinear periodic response characteristics of oval cylindrical shells are investigated using the finite strip method. The governing equations are solved by the shooting technique, coupled with the Newmark time marching scheme and the arc length continuation algorithm.

The influence of ovality parameter and loading location on the periodic response is studied in detail. It is found that for the circular shells, all modes with close linear free vibration frequencies are excited due to the concentrated harmonic excitation force.

With an increase in ovality parameter, the nonlinear dynamic response changes significantly, due to increased modal interactions and participation of higher harmonics. The AS and SS modes participate in the response corresponding to primary branch of symmetrically excited noncircular shells.

For nonsymmetrically excited shells and in the secondary branch of symmetrically excited shells, all the modes participate in the nonlinear response. Due to 1:1 internal resonance between AS/SS and SA/AA modes, a secondary branch emanating from primary one through the symmetry breaking bifurcation is predicted for symmetrically excited oval shell with $\zeta = 0.6$.

For symmetrically excited oval shells, waves travelling in one direction from loading point in secondary branch of the response curve are predicted.

For nonsymmetrically excited oval shells ($\zeta = 0.6$), either waves moving in anticlockwise direction from the loading point ($y^* = 3C/16$) or those originating near major axis ($y = 0$) moving in opposite directions in the top and bottom halves of the shell are observed in certain forcing frequency range.

The traveling waves in earlier work are due to driven and companion modes with a specific circumferential wave number, whereas the contribution of several modes is responsible for the traveling wave behavior predicted in the present work.

List of symbols

\cdot_0	Middle surface/magnitude	N	Number of degrees of freedom
α, β	Rayleigh damping parameters	\cdot_n	Circumferential wave number
A, B	Stiffness coefficient matrices	\tilde{N}	Stress resultant vector
\cdot_b	Bending component	\cdot^{NL}	Nonlinear
C	Circumference	\bar{N}_k^0	Original shape function
D, E	Stiffness coefficient matrices	\bar{N}_k^1	Smoothed shape function
$\ddot{\delta}, \dot{\delta}, \delta$	Acceleration, velocity and displacement vectors	ν	Poisson's ratio
E	Young's modulus	ω_{mn}	Linear free vibration frequency
ϵ	Strain vector	ω_F	Forcing frequency
η	State vector	ω_i	Frequency of the i -th harmonic
F	Discrete force	\cdot_p	Extensional/stretching component
F	Force vector	\tilde{Q}	Transverse shear stress resultant vector
h	Thickness	r	Radius of curvature
I	Rotary inertia	r_0	Average radius of curvature ($= C/2\pi$)
K	Constant stiffness matrix	ρ	Density
K_1, K_2	Stiffness matrices linearly and quadratically dependent on field variables	t	Time
L	Meridional length	T	Time period
\cdot^L	Linear	\tilde{T}	Kinetic energy
\cdot_m	Number of half sine waves in meridional direction	θ_x, θ_y	Rotation of meridional and circumferential sections
M	Number of terms in the displacement fields in the meridional direction	U	Total potential energy
M	Consistent mass matrix	u, v, w	Displacements in meridional, circumferential and thickness directions
\tilde{M}	Moment resultant vector	x, y, z	Coordinate directions
		ξ	Damping parameter
		y^*	Circumferential location of discrete harmonic load
		ζ	Ovality parameter

References

- [Amabili 2003] M. Amabili, "A comparison of shell theories for large-amplitude vibrations of circular cylindrical shells: Lagrangian approach", *J. Sound Vib.* **264**:5 (2003), 1091–1125.
- [Amabili 2008] M. Amabili, *Nonlinear vibrations and stability of shells and plates*, Cambridge University Press, New York, 2008.
- [Amabili and Païdoussis 2003] M. Amabili and M. P. Païdoussis, "Review of studies on geometrically nonlinear vibrations and dynamics of circular cylindrical shells and panels, with and without fluid-structure interaction", *Appl. Mech. Rev. (ASME)* **56**:4 (2003), 349–381.
- [Babu and Prathap 1986] C. R. Babu and G. Prathap, "A linear thick curved beam element", *Int. J. Numer. Methods Eng.* **23**:7 (1986), 1313–1328.
- [Ibrahim et al. 2008a] S. M. Ibrahim, B. P. Patel, and Y. Nath, "Large amplitude vibrations of noncircular cylindrical shells", pp. 173–188 in *Vibration problems ICOVP-2007* (Shibpur, India, 2007), edited by E. Inan et al., Springer Proceedings in Physics **126**, 2008.

- [Ibrahim et al. 2008b] S. M. Ibrahim, B. P. Patel, and Y. Nath, "On the nonlinear vibrations of clamped oval shells", pp. 645–652 in *Proceedings of Ninth Biennial ASME Conference on Engineering Systems Design and Analysis*, vol. 1 (or CD-ROM), 2008.
- [Ibrahim et al. 2009] S. M. Ibrahim, B. P. Patel, and Y. Nath, "Modified shooting approach to the non-linear periodic forced response of isotropic/composite curved beams", *Int. J. Non-Linear Mech.* **44**:10 (2009), 1073–1084.
- [Ibrahim et al. 2010] S. M. Ibrahim, B. P. Patel, and Y. Nath, "Nonlinear periodic response of composite curved beam subjected to symmetric and antisymmetric mode excitation", *J. Comput. Nonlinear Dynam. (ASME)* **5**:2 (2010), #021009.
- [Kozarov and Mladenov 1979] M. Kozarov and K. Mladenov, "Nonlinear vibrations of elliptic cylindrical shells", *Akad. Nauk SSSR Izv. Mekh. Tverd. Tela* **5** (1979), 144–151. In Russian.
- [Moussaoui and Benamar 2002] F. Moussaoui and R. Benamar, "Non-linear vibrations of shell-type structures: a review with bibliography", *J. Sound Vib.* **255**:1 (2002), 161–184.
- [Nayfeh and Balachandran 1994] A. H. Nayfeh and B. Balachandran, *Applied nonlinear dynamics: analytical, computational, and experimental methods*, Wiley, New York, 1994.
- [Padmanabhan and Singh 1995] C. Padmanabhan and R. Singh, "Analysis of periodically excited non-linear systems by a parametric continuation technique", *J. Sound Vib.* **184**:1 (1995), 35–58.
- [Pandalai and Sathyamoorthy 1970] K. A. V. Pandalai and M. Sathyamoorthy, "Nonlinear flexural vibrations of orthotropic oval cylindrical shells", pp. 47–74 in *Studies in structural mechanics: to honour N. J. Hoff*, edited by K. A. V. Pandalai, 1970.
- [Patel et al. 2002] B. P. Patel, M. Ganapathi, D. P. Makhecha, and S. S. Gupta, "On the nonlinear free flexural vibrations problem for thin elastic rings", *J. Aeronaut. Soc. India* **54** (2002), 298–309.
- [Patel et al. 2003] B. P. Patel, M. Ganapathi, D. P. Makhecha, and P. Shah, "Large amplitude free flexural vibration of rings using finite element approach", *Int. J. Non-Linear Mech.* **38**:6 (2003), 911–921.
- [Patel et al. 2009] B. P. Patel, S. M. Ibrahim, and Y. Nath, "Periodic response of nonlinear dynamical system with large number of degrees of freedom", *Sadhana* **34**:6 (2009), 1033–1037.
- [Rajasekaran and Murray 1973] S. Rajasekaran and D. W. Murray, "Incremental finite element matrices", *J. Struct. Div. (ASCE)* **99**:12 (1973), 2423–2338.
- [Ribeiro 2004] P. Ribeiro, "Non-linear forced vibrations of thin/thick beams and plates by the finite element and shooting methods", *Comput. Struct.* **82**:17-19 (2004), 1413–1423.
- [Ribeiro 2008] P. Ribeiro, "Forced large amplitude periodic vibrations of cylindrical shallow shells", *Finite Elem. Anal. Des.* **44**:11 (2008), 657–674.
- [Soedel 1993] W. Soedel, *Vibrations of shells and plates*, 2nd ed., Dekker, New York, 1993.
- [Soldatos 1999] K. P. Soldatos, "Mechanics of cylindrical shells with non-circular cross-section: a survey", *Appl. Mech. Rev. (ASME)* **52**:8 (1999), 237–274.
- [Sundararajan and Noah 1997] P. Sundararajan and S. T. Noah, "Dynamics of forced nonlinear systems using shooting/arc-length continuation method: application to rotor systems", *J. Vib. Acoust. (ASME)* **119**:1 (1997), 9–20.

Received 28 Jan 2010. Revised 29 Apr 2010. Accepted 8 May 2010.

SYED MUHAMMAD IBRAHIM: ibrahimmail@rediffmail.com

Department of Applied Mechanics, Indian Institute of Technology Delhi, Hauz Khas, New Delhi 110016, India

BADRI PRASAD PATEL: badripatel@hotmail.com

Department of Applied Mechanics, Indian Institute of Technology Delhi, Hauz Khas, New Delhi 110016, India

YOGENDRA NATH: nathyogendra@hotmail.com

Department of Applied Mechanics, Indian Institute of Technology Delhi, Hauz Khas, New Delhi 110016, India

JOURNAL OF MECHANICS OF MATERIALS AND STRUCTURES

<http://www.jomms.org>

Founded by Charles R. Steele and Marie-Louise Steele

EDITORS

CHARLES R. STEELE Stanford University, U.S.A.
DAVIDE BIGONI University of Trento, Italy
IWONA JASIUK University of Illinois at Urbana-Champaign, U.S.A.
YASUhide SHINDO Tohoku University, Japan

EDITORIAL BOARD

H. D. BUI École Polytechnique, France
J. P. CARTER University of Sydney, Australia
R. M. CHRISTENSEN Stanford University, U.S.A.
G. M. L. GLADWELL University of Waterloo, Canada
D. H. HODGES Georgia Institute of Technology, U.S.A.
J. HUTCHINSON Harvard University, U.S.A.
C. HWU National Cheng Kung University, R.O. China
B. L. KARIHALOO University of Wales, U.K.
Y. Y. KIM Seoul National University, Republic of Korea
Z. MROZ Academy of Science, Poland
D. PAMPLONA Universidade Católica do Rio de Janeiro, Brazil
M. B. RUBIN Technion, Haifa, Israel
A. N. SHUPIKOV Ukrainian Academy of Sciences, Ukraine
T. TARNAI University Budapest, Hungary
F. Y. M. WAN University of California, Irvine, U.S.A.
P. WRIGGERS Universität Hannover, Germany
W. YANG Tsinghua University, P.R. China
F. ZIEGLER Technische Universität Wien, Austria

PRODUCTION

PAULO NEY DE SOUZA Production Manager
SHEILA NEWBERY Senior Production Editor
SILVIO LEVY Scientific Editor

Cover design: Alex Scorpan


Cover photo: Ev Shafirir

See inside back cover or <http://www.jomms.org> for submission guidelines.

JoMMS (ISSN 1559-3959) is published in 10 issues a year. The subscription price for 2010 is US \$500/year for the electronic version, and \$660/year (+\$60 shipping outside the US) for print and electronic. Subscriptions, requests for back issues, and changes of address should be sent to Mathematical Sciences Publishers, Department of Mathematics, University of California, Berkeley, CA 94720-3840.

JoMMS peer-review and production is managed by EditFLOW™ from Mathematical Sciences Publishers.

PUBLISHED BY

 **mathematical sciences publishers**
<http://www.mathscipub.org>

A NON-PROFIT CORPORATION

Typeset in L^AT_EX

©Copyright 2010. Journal of Mechanics of Materials and Structures. All rights reserved.

A semianalytical solution for the bending of clamped laminated doubly curved or spherical panels	
KASRA BIGDELI and MOHAMMAD MOHAMMADI AGHDAM	855
Analytical solution for a concentrated force on the free surface of a coated material	
ZHIGEN WU, YIHUA LIU, CHUNXIAO ZHAN and MEIQIN WANG	875
On the nonlinear dynamics of oval cylindrical shells	
S. M. IBRAHIM, B. P. PATEL and Y. NATH	887
Time-harmonic elastodynamic Green's function for the half-plane modeled by a restricted inhomogeneity of quadratic type	
TSVIATKO V. RANGELOV and GEORGE D. MANOLIS	909
An enhanced asymptotic expansion for the stability of nonlinear elastic structures	
CLAUS DENCKER CHRISTENSEN and ESBEN BYSKOV	925
Stress and strain recovery for the in-plane deformation of an isotropic tapered strip-beam	
DEWEY H. HODGES, ANURAG RAJAGOPAL, JIMMY C. HO and WENBIN YU	963
Assessment of the performance of uniform monolithic plates subjected to impulsive loads	
JONAS DAHL	977
Stress smoothing holes in planar elastic domains	
SHMUEL VIGDERGAUZ	987
Numerical simulation of failed zone propagation process and anomalies related to the released energy during a compressive jog intersection	
XUE-BIN WANG, JIN MA and LI-QIANG LIU	1007
Revisiting the Hult–McClintock closed-form solution for mode III cracks	
ZHI-JIAN YI	1023